Supporting Information

Vanguri et al. 10.1073/pnas.1208328110

SI Materials and Methods

Virus, Tetramers, and Infections. IA^b–3K and IA^b–3K APL tetramers were constructed as described previously (1). Vac expressing $IA^b\beta$-linked peptide and peptides fused to the carboxyl termini of GFP were constructed using standard techniques. Mice were infected i.p. with 10^7 pfu of recombinant vaccinia viruses.

In Vitro T-Cell Activation and Intracellular Cytokine Production. T-cell activation in vitro was assessed by incubating 3×10^5 naïve $Rag1^{-/-}$ B3K506 or B3K508 $CD4^+$ T cells for 4 h with 1×10^5 bone marrow-derived dendritic cells (BM-DCs) infected with either Vac:IA^b–peptide or Vac:peptide–GFP viruses in the presence of GolgiStop and GolgiPlug (1 μL/mL; BD Biosciences). T cells were then surfaced stained with anti-CD4 and anti-CD8, washed, fixed in 2% (vol/vol) formaldehyde, and stained for intracellular TNFα using a Cytofix/Cytoperm kit (BD Biosciences) using the manufacturer's protocol. TNFα expression by $CD4^+$ T cells was assessed using flow cytometry (FACSCaliber; BD Biosciences) and analyzed using FlowJo Version 8.3 (TreeStar). BM-DCs were differentiated in vitro by growing BM with GM-CSF for 7 d following standard procedures. BM-DCs were then infected with Vac viruses at a multiplicity of infection (MOI) of 3 for 12 h before incubation with CD4 T cells.

To analyze CD4 T-cell responses in 506β mice following Vac infection, 5×10^6 spleen cells were pulsed with titrating concentrations of 3K or APLs in the presence of GolgiStop and GolgiPlug (1 μL/mL; BD Biosciences) for 5 h at 37 °C, then cell surfaced stained, fixed, and stained for intracellular TNFα and IFNγ expression. In some experiments, IA^b–3K, –P-1A, –P-1L, or –P-1K tetramers were added during the last 2 h of stimulation at a final concentration of 10 μg/mL.

Tetramer and Antibody Stains. Spleen cells (5×10^6) from Vac-infected mice were incubated with anti-Fc receptor antibody 2.4G2, then stained with 10 μg/mL either IA^b–3K, –P-1A, –P-1L, or –P-1K tetramer for 90 min at 37 °C. Cells were washed and stained with antibodies specific for Thy1.2, CD4, CD8, B220, and CD44. In some experiments, these cells were also stained with antibodies specific for CD69, CD25, and ICOS or analyzed for the dilution of carboxyfluorescein succinimidyl ester dye.

Adoptive-Transfer Experiments. B3K506 or B3K508 CD4 T cells (1×10^5) were transferred i.v. into congenically marked C57BL/6.SJL ($CD45.1^+$) mice. Mice were infected with 10^7 pfu vaccina virus 2 h after T-cell transfer, and the responding CD4 T cells were analyzed at 18 h, 48 h, 7 d, or 28 d postinfection.

EC_{50} Determination. Each dose–response curve was scaled such that the responses at no stimulation and 10 mm were 0 and 1, respectively, assuming saturation by 10 mM. The concentration at which the response was half-maximal (EC_{50}) was determined by linear interpolation after log-transforming the peptide concentration.

Estimating the Potency and, thus, the Relative Concentration of Viral–pMHC Complexes Displayed Following Infections. Two sets of recombinant vaccinia viruses (Vac) were constructed. One set of viruses expresses the foreign-antigen peptide, 3K, or 3K APLs (peptides derived from the wild-type peptide sequence that carry individual amino acid substitutions) fused to GFP (Vac:3K–GFP). The other set expresses the same 3K or 3K APL peptides fused to the carboxyl termini of the MHCII, $IA^b\beta$ chain (Vac:IA^b–3K) (Fig. S1 *A* and *B*). The two sets were expected to produce, on infected APCs, different densities of viral pMHC complexes. The soluble peptide versions of the 3K APL used in this study have strong, medium, and weak abilities to activate the 3K-reactive, B3K506 and B3K508 CD4 T cells (2). For example, the soluble 3K peptide has a strong potency to activate B3K506 CD4 T cells, requiring only 3 nM soluble 3K peptide loaded onto BM-DCs to induce the half-maximal amount of TNFα expression (TNFα EC_{50}). In contrast, the medium-potency 3K, P-1A APL and the weak-potency 3K, P-1K APL require 68 nM and 5,500 nM soluble peptide, respectively, to induce half-maximal TNFα expression. For the B3K508 CD4 T cells, the soluble 3K peptide has a strong potency requiring only 6 nM soluble peptide to induce half-maximal TNFα expression, whereas the medium potency 3K APL, P5R, requires 87 nM soluble peptide for a similar induction of TNFα [see table S1 by Govern et al. (2) for a complete list of APL and the EC_{50} values of TNFα expression and in vitro proliferation for naïve B3K506 and B3K508 CD4 T cells].

We observed that naïve B3K506 and B3K508 CD4 T cells always produced equal or greater amounts of TNFα in vitro when challenged with BM-DCs infected with Vac:IA^b–peptide viruses compared with BM-DCs infected with Vac:peptide–GFP viruses expressing the same 3K APL (Fig. S1 *C* and *D*). B3K506 and B3K508 CD4 T cells incubated with C57BL/6-derived, Vac:IA^b–3K– or Vac:3K–GFP–infected BM-DCs induced maximal amounts of TNFα. These data indicate that both Vac:3K–GFP– and Vac:IA^b–3K–infected BM-DCs create and present enough IA^b+3K complexes on the cell surface to fully activate the B3K506 and B3K508 CD4 T cells in this in vitro assay. In contrast, BM-DCs infected with the Vac:IA^b–peptide viruses Vac:IA^b–P-1A, Vac:IA^b–P-1K, or Vac:IA^b–P8A induce more TNFα production from B3K506 CD4 T cells than BM-DCs infected with the corresponding Vac:peptide–GFP viruses, Vac:P-1A–GFP, Vac:P-1K–GFP, or Vac:P8A–GFP (Fig. S1*C*). Similarly, Vac:IA^b–P5R– and Vac:IA^b–P8R–infected BM-DCs induce more TNFα production from B3K508 CD4 T cells compared with BM-DCs infected with the corresponding Vac:peptide–GFP viruses, Vac:P5R–GFP or Vac:P8R–GFP (Fig. S1*D*). These data indicate that BM-DCs infected with Vac:IA^b–peptide viruses create enough viral pMHC complexes displayed on the cell surface such that even weak and medium potency peptides are able to induce TNFα expression from B3K506 or B3K508 CD4 T cells. In contrast, BM-DCs infected with the matching Vac:peptide–GFP virus did not create enough viral pMHC complexes displayed on the cell surface to induce an equivalent level of TNFα expression when the peptides were of weak or medium potency.

The in vitro TNFα production assay uses purified CD4 T cells mixed with infected BM-DCs for a short incubation time (4 h), with a 3:1 ratio of CD4 T cells and BM-DCs. Thus, the assay primarily tests the ability of BM-DCs to directly present pMHC complexes at a sufficient level to activate T cells and occurs in the absence of most indirect effects on T-cell activation that can occur during in vivo immune responses that may confound the readout, such as T-cell competition or T-cell differentiation. Because in vitro T-cell activation assays are strongly sensitive to antigen concentration, the greater potency of BM-DCs infected with Vac:IA^b–P-1A, Vac:IA^b–P-1K, and Vac:IA^b–P8A versus Vac:P-1A–GFP, Vac:P-1K–GFP, and Vac:P8A–GFP to activate B3K506 CD4 T cells, for example, strongly suggests that BM-DCs infected with Vac:IA^b–peptide viruses create a higher

density of viral pMHC complexes on the cell surface compared with BM-DCs infected with Vac:peptide–GFP viruses.

We sought to estimate the difference in the potency of BM-DCs infected with Vac:IA^b–peptide versus Vac:peptide–GFP viruses and, thus, the relative concentration of viral pMHC complexes displayed following infections. A previous study determined how the T cells in our study respond to increasing concentrations of various soluble peptide ligands (2). Our current study determined how the CD4 T cells respond to BM-DCs infected with vaccinia viruses that express these same peptides. We could, therefore, estimate the concentration of soluble ligand (3K or 3K APL) required to produce the same response as BM-DCs infected with each virus; we called this the "equivalent soluble ligand concentration" for infection. To facilitate this estimation, we modeled the dose–response curves previously obtained from experiments with soluble ligand as sigmoidal curves:

$$\frac{r}{r_{\max}} = \frac{1}{1 + (c/EC_{50})^{-N}} \qquad \textbf{[S1]}$$

where r is the TNFα response to a concentration, c, of a soluble ligand. The parameters N and $r_{\max}$, assumed to be the same for all peptide-TCR interactions, describe how sensitively the response depends on the concentration and the maximal TNFα response at saturating concentrations of peptides, respectively.

We assumed that the equivalent soluble ligand concentrations are the same for all ligands introduced with either Vac:peptide–GFP infections (c_{GFP}) or Vac:IA^b–peptide infections (c_{IAb}). This assumption is consistent with previous studies that have shown several of the peptides bind IA^b within a twofold difference (3); the rest of the APLs have substitutions at the same, non-MHC anchor residues. We then used Eq. **S1** with measured TNFα responses following infection, r, and EC_{50} values fit from soluble ligand experiments for each pMHC–TCR interaction to simultaneously fit the equivalent soluble ligand concentrations, c_{GFP} and c_{IAb}, the maximal response, $r_{\max}$, and the sensitivity, N, for our experiments in this study (Fig. S1*E*).

The resulting fit parameters were $n = 1$, $r_{\max} = 60\%$, $c_{\mathrm{GFP}} = 35$ nM, and $c_{\mathrm{IAb}} = 2{,}100$ nM. Note that the fit value for N agrees well with the soluble ligand dose–response curves, a check on the model; the parameter $r_{\max}$ is expected to vary across experiments (Fig. S1*F*). The ratio of equivalent soluble ligand concentrations, $c_{\mathrm{IAb}}/c_{\mathrm{GFP}}$, is ∼100. If it is assumed that soluble peptides are loaded onto MHC molecules proportionally to their concentration in solution within the experimental concentration range, the 3K and 3K APL peptides are presented at approximately a 100-fold higher density on the surface of APCs infected with Vac:IA^b–3K, compared with Vac:3K–GFP viruses.

Why might BM-DCs infected with Vac:IA^b–peptide viruses create more viral pMHC displayed on the cell surface than those infected with Vac:peptide–GFP viruses? Within the primary infected APC, several aspects of cellular processing and presentation may impact the level of viral pMHC presentation. First, Vac:IA^b–peptide infections may create more 3K peptide available to be presented. It is possible that Vac:IA^b–peptide infection produces more IA^b–peptide fusion protein than Vac:peptide–GFP infection produces peptide–GFP fusion proteins. Second, the Vac:3K–GFP viruses produce a fusion protein which requires the 3K peptide to be cleaved and transported into the endosome/lysosome by cellular machinery before being loaded onto MHC molecules and trafficking to the cell surface. In contrast, Vac:IA^b–3K infection produces IA^{b}β–3K fusion proteins that can directly pair with endogenous IA^{b}α chains to form a complete pMHC complex and be transported to the cell surface (4). This may allow the same amount of 3K peptide created following Vac:IA^b–3K infections to be more efficiently displayed as a pMHC complex on the cell surface, compared with 3K peptide produced following Vac:3K–GFP infections. Third, the IA^b–peptide fusion protein has a linker between the peptide and the MHCβ chain. Although this linker is often cleaved in APCs that express the invariant chain, some cell surface-expressed viral pMHC may continue to have the peptide linked to the IA^{b}β chain (4). Having an MHC-linked peptide could allow the same peptide, if it is released from the MHC, to rebind the same MHC and, thus, extend the lifetime of the pMHC complex. All three mechanisms could result in a greater level of viral pMHC complex displayed on the cell surface.

Summary of the TCR–pMHC Confinement-Time Model for the Activation of CD4 T Cells. T-cell activation has been extensively studied in vitro and in vivo and the potency of pMHC ligands has been primarily ascribed to the $t_{1/2}$ or the K_D of the TCR–pMHC interaction. By studying pMHC ligands that have different K_D and binding kinetics, we and others have found that ligand potency measured in in vitro assays does not always follow a strict $t_{1/2}$ or K_D model of activation (2, 3). We found that for individual CD4 T cells, ligand potency followed the overall trend of both K_D- and $t_{1/2}$-based models. However, when we compared the activation profiles of multiple CD4 T cells (B3K506 and B3K508 T cells) with several defined pMHC ligands (3K and APL variants), neither model sufficed (2).

In regards to the K_D model of activation, B3K508 CD4 T cells are activated too well. For example, the B3K506 and B3K508 TCRs interact with the IA^b+3K complex with differing K_D (7 μM for the B3K506; 29 μM for the B3K508), and yet naïve B3K506 and B3K508 CD4 T cells proliferate and produce TNFα in response to similar titrating concentrations of soluble 3K peptide in vitro. In another example, the B3K506 TCR binds IA^b+P-1A (26 μM) with similar K_D as the B3K508 TCR binding to IA^b+3K (29 μM), and yet B3K506 CD4 T cells proliferate at an EC_{50} that is 23-fold less than B3K508 T cells. These and other previously tested 3K APLs indicated that the K_D of a TCR–pMHC interaction does not define the ligand potency.

Similarly, ligand potency measured using in vitro assays did not correlate with the $t_{1/2}$ because B3K506 CD4 T cells are activated too well. B3K506 CD4 T cells ($t_{1/2}$ = 0.9 s) and B3K508 CD4 T cells ($t_{1/2}$ = 2.2 s) proliferate and produce TNFα in vitro in response to similar concentrations of soluble 3K peptide and yet have different $t_{1/2}$. Additional discrepancies were observed when comparing other 3K APLs, including the demonstration that the P5R ligand is significantly less potent at activating B3K508 CD4 T cells than the 3K ligand is at activating B3K506 CD4 T cells, despite having a similar $t_{1/2}$ (0.7 and 0.9 s, respectively).

We consistently observed that the activating ligands for B3K506 T cells used fast on-rates to create a strong K_D and that this was compensating for short $t_{1/2}$. Vice versa, the B3K508 T cells engage IA^b+3K ligands with a longer $t_{1/2}$, which allows pMHC ligands with weaker K_D to be highly potent. Collectively, these findings suggested to us that the potency of a pMHC ligand is determined by an interplay between the on-rate and $t_{1/2}$ (or K_D and $t_{1/2}$) of the TCR–pMHC interactions, in a way that allows fast-kinetic ligands to have enhanced signaling properties.

In an attempt to reconcile how the interplay of K_D and binding kinetics influences T-cell activation, we analyzed our in vitro ligand-potency data within the context of several potential models. These included whether serial triggering or TCR–pMHC occupancy when TCR and pMHC are membrane-bound could explain our dataset; see SI text by Govern et al. (2) for a complete analysis of the tests, estimations, and assumptions used to convert the equilibrium affinity and binding kinetics of TCR–pMHC interactions measured in solution to those that are anchored onto membranes. These analyses indicated that ligand potency models based on K_D (receptor occupancy), $t_{1/2}$, or serial-triggering models did not fit our dataset.

Another model, TCR–pMHC confinement time, was found to best predict the activation of CD4 T cells in vitro. The confinement-time model is a TCR–pMHC kinetic model that incorporates rebinding: the ability of an individual receptor/ligand pair to associate, disassociate, and reassociate in a finite amount of time before complete disengagement (2, 3, 5). Although TCR–pMHC interactions are usually thought of as single binding events, TCR/ligand pairs with fast on-rates may be able to rebind (6), especially because they are bound on membranes where diffusivities are typically slower than in solution. TCR–pMHC rebinding would create an aggregate dwell time of interaction (the confinement time), t_a, assuming the rebindings occur faster than the TCR signaling-complex disassembles.

The t_a (aggregate dwell time or confinement time) depends on both the $t_{1/2}$, which determines the duration of any individual binding interaction, and the k_{on}, which determines how many times an individual TCR and pMHC rebind before diffusing away from each other. In addition, the t_a depends on a threshold on-rate for rebindings, k^*_{on}. TCR–pMHC pairs with on-rates faster than this threshold are predicted to rebind at least once. Further increases in the on-rate allow rebinding to occur more often than TCR–pMHC pairs with slower on-rates. The t_a has a qualitatively different dependence on the $t_{1/2}$ and k_{on} when on-rates are slow versus fast. When on-rates are fast relative to the membrane diffusion rates, pMHC binds and rebinds the same TCR many times reaching a quasiequilibrium before diffusing away. This causes the equilibrium affinity (a simple function of the k_{on} and $t_{1/2}$) to become the dominant factor that determines the t_a of the interaction. However, when on-rates are slow, rebinding does not occur and the t_a equals the $t_{1/2}$ of an individual TCR–pMHC engagement.

TCR–pMHC confinement-time models predict that ligand potency is dependent upon the aggregate dwell time of interaction and not just the $t_{1/2}$ of an individual TCR–pMHC engagement. In essence, the TCR–pMHC confinement-time model incorporates TCR–pMHC rebinding within a standard $t_{1/2}$ model.

Our TCR–pMHC t_a model was generated without empirically fitting the B3K506 or B3K508 CD4 T-cell activation data. The rebinding threshold, the only parameter in the model, was predicted to be ~60,000/(M × s), based on experimentally measured biophysical parameters. In comparing the model to the activation profiles of B3K506 and B3K508 CD4 T cells responding to strong-potency ligands, we found that 60,000/(M × s) is near the best fit for minimizing the variation in the aggregate $t_{1/2}$. Quite similarly, for medium-potency ligands, the best-fit threshold was found to be ~45,000/(M × s). The ability of the TCR–pMHC confinement-time model to predict the in vitro potency of CD4 T-cell ligands, in which there is a variance of k_{on}, k_{off}, and K_D, suggests the assumptions and underlying biophysical mechanisms are correct. Furthermore, direct evidence of rebinding has been observed between membrane-bound CD2 and CD58 using Fluorescence recovery after photobleaching (FRAP), as well as Src homology 2-containing proteins near the plasma membrane, indicating that fast-binding receptor ligand pairs can have significant increases in the duration of the bonds (7–9).

Statistical Analysis of Whether Antiviral CD4 T-Cell Responses in Vivo Correlate Best with the K_D, $t_{1/2}$, or t_a of the Viral pMHC–TCR Interaction. How well CD4 T-cell activation profiles generated using in vitro assays correlate with in vivo CD4 T-cell responses to viral infection is unclear. To elucidate whether antiviral CD4 T-cell burst size is predicted by specific biophysical parameters of the TCR–pMHC interaction, we compared the clonal burst size and maintenance of B3K508 and B3K506 T cells responding to each infection with the previously measured TCR–pMHC K_D, $t_{1/2}$, or calculated t_a. This allowed for three groups of T-cell responses to be compared based on whether the TCR–pMHC interaction has a similar K_D, $t_{1/2}$, or calculated t_a (Table S1) (2). The t_a was calculated using two values for the threshold on-rate for rebinding, k^*_{on} [k^*_{on} = 60,000/(M × s); and k^*_{on} = 45,000/(M × s)], because these values correspond to our theoretically derived value and our empirically derived, best-fit value for the threshold on-rate for rebinding (Table S1). Using different values of k^*_{on} models the uncertainties in different parameters that affect k^*_{on}, including the diffusivities of the TCR and the pMHC, and the conversion from SPR-measured k_{on} to k_{on} on the membrane. It is also a rough way of accounting for other factors that might increase or decrease the likelihood of rebinding, such as membrane motion; see Govern et al. for a complete description of the calculation (2).

We used three different statistical analyses to determine whether TCR–pMHC K_D, $t_{1/2}$, or calculated t_a best predicts CD4 T-cell responses in vivo. The first analysis, in the main text, involved analyzing groups of similar K_D, $t_{1/2}$, or calculated t_a for outliers. As a second analysis, we used a simple linear regression to determine how strongly the burst size is correlated with the different parameters. This method of analysis has been used previously to evaluate confinement-time models (10). The third analysis used a mutual information metric to allow for possible nonlinear relationships between the burst size and the kinetic parameters. Using all methods, we found that the calculated t_a was the best predictor of CD4 T cells responding to viral infections.

Using a linear regression analysis of the size of the T-cell response after infection with Vac:peptide–GFP viruses, we found an r^2 value for t_a [k^*_{on} = 60,000/(M × s)] to be 0.76 for the burst size and 0.75 during the maintenance phase, and for t_a [k^*_{on} = 45,000/(M × s)] to be 0.82 for the burst size and 0.85 during the maintenance phase (Fig. 5). In contrast, the r^2 values for $t_{1/2}$ are 0.34 for the burst size and 0.25 during the maintenance phase, whereas the r^2 values for K_A are 0.42 for the burst size and 0.55 during the maintenance phase. Thus, T-cell response correlates most strongly with t_a. The results for infection with Vac:IA^b–3K are similar but do not strongly discriminate between K_A and t_a models (Fig. S4).

In general, the relationship between burst size and the different kinetic parameters may be nonlinear (e.g., doubling t_a may more than double the burst size or it may less than double it). To analyze the data in way that allows for possible nonlinearities, we compared the mutual information between K_A, $t_{1/2}$, or t_a and the burst size, rather than the correlation coefficient as in the linear analysis. The mutual information between two variables is a measure of how well knowing one variable provides information about the value of the other (11). For example, if K_A were the only biophysical parameter that determines burst size, then we would expect knowing the value of K_A to enable us to predict the burst size accurately, except for some uncertainty that comes from other confounding factors and the intrinsic stochasticity of the T-cell response to stimulation. The correlation coefficient also measures how well knowing a parameter enables prediction of the response, but it forces linear predictions. In contrast, mutual information does not make an assumption about the functional relationship between variables (12).

To calculate mutual information, we binned the data according to the independent (K_A, $t_{1/2}$, or t_a) and log-transformed dependent (T-cell expansion) variables. Because the amount of data are limited, we chose three bins for each. We then calculated mutual information as:

$$I(X;Y) = \sum_{i=1}^{3}\sum_{j=1}^{3} p_{ij} \ln \frac{p_{ij}}{p_{i\text{-}}p_{\text{-}j}} \qquad \text{[S2]}$$

where $X = K_A$, $t_{1/2}$, or t_a; Y is the response; $p_{i\text{-}}$ is the fraction of data points that falls in the ith bin of the independent variable

(K_A, $t_{1/2}$, or t_a); $p_{\cdot j}$ is the fraction that falls in the jth bin of the dependent variable (the response); and p_{ij} is the fraction that falls in both the ith independent variable bin and the jth dependent variable bin. The parameters $p_{i\cdot}$, $p_{\cdot j}$, and p_{ij} summarize the data by describing how much of it falls in different ranges of the independent and dependent variables. Higher values of the mutual information $I(X;Y)$ correspond to noiseless relationships between X and Y, whereas scores that tend to 0 are statistically independent variables (12).

The best possible mutual information score for any of the independent variables is 0.64 nats, the entropy (self-information) of the response variable at this level of binning. The unit "nats" indicates that the logarithm in Eq. **S2** is a natural logarithm. This maximum score reflects the fact that there are only three possible values of the response at the level of our binning, so knowing the value of K_A, $t_{1/2}$, or t_a can decrease our uncertainty about the response, at most, by removing two possibilities for the bin in which it falls. For the response to Vac:peptide–GFP infections at day 7, the information contents of K_A, $t_{1/2}$, t_a [k^*_{on} = 45,000/(M × s)] and t_a [(k^*_{on} = 60,000/(M × s)] were 50%, 27%, 100%, and 100% of the maximum, respectively. Thus, t_a contains the maximal possible information at this level of binning. The results corroborate the conclusion that the confinement time is the best explanatory variable for the clonal burst size of CD4 T cells responding to vaccinia infections, although the significance of the metric is limited by the size of the datasets. Increasing or decreasing the number of bins resulted in too many data points falling in separate bins of the dependent or independent variable or too many data points falling in the same bin, compromising the statistics. However, for bin numbers in the range of 1–5, K_D or $t_{1/2}$ never provided more information about the response than the confinement time. For the response at 28 d to Vac:peptide–GFP infections, the results were similar: the information content of K_A, $t_{1/2}$, t_a [k^*_{on} = 45,000/(M × s)] and t_a [k^*_{on} = 60,000/(M × s)] were 50%, 27%, 100%, and 100% of the maximum, respectively. Collectively, using three different statistical tests that differ in the scale at which they analyze the data, and in their assumptions about linearity of the relationship between the kinetic variables and the response, t_a was found to be the best predictor of primary CD4 T-cell responses.

1. Huseby ES, Crawford F, White J, Marrack P, Kappler JW (2006) Interface-disrupting amino acids establish specificity between T cell receptors and complexes of major histocompatibility complex and peptide. *Nat Immunol* 7(11):1191–1199.
2. Govern CC, Paczosa MK, Chakraborty AK, Huseby ES (2010) Fast on-rates allow short dwell time ligands to activate T cells. *Proc Natl Acad Sci USA* 107(19):8724–8729.
3. Liu XQ, et al. (2002) Alternate interactions define the binding of peptides to the MHC molecule IA(b). *Proc Natl Acad Sci USA* 99:8820–8825.
4. Ignatowicz L, Winslow G, Bill J, Kappler J, Marrack P (1995) Cell surface expression of class II MHC proteins bound by a single peptide. *J Immunol* 154(8):3852–3862.
5. Valitutti S, Coombs D, Dupré L (2010) The space and time frames of T cell activation at the immunological synapse. *FEBS Lett* 584(24):4851–4857.
6. Dushek O, Das R, Coombs D (2009) A role for rebinding in rapid and reliable T cell responses to antigen. *PLOS Comput Biol* 5(11):e1000578.
7. Tolentino TP, et al. (2008) Measuring diffusion and binding kinetics by contact area FRAP. *Biophys J* 95(2):920–930.
8. Kaizuka Y, Douglass AD, Vardhana S, Dustin ML, Vale RD (2009) The coreceptor CD2 uses plasma membrane microdomains to transduce signals in T cells. *J Cell Biol* 185(3): 521–534.
9. Oh D, et al. (2012) Fast rebinding increases dwell time of Src homology 2 (SH2)-containing proteins near the plasma membrane. *Proc Natl Acad Sci USA* 109(35): 14024–14029.
10. Dushek O, et al. (2011) Antigen potency and maximal efficacy reveal a mechanism of efficient T cell activation. *Sci Signal* 4(176):ra39.
11. Cover TM, Thomas JA (2006) *Elements of Information Theory* (Wiley-Interscience, Hoboken, NJ), 2nd Ed.
12. Reshef DN, et al. (2011) Detecting novel associations in large data sets. *Science* 334(6062):1518–1524.

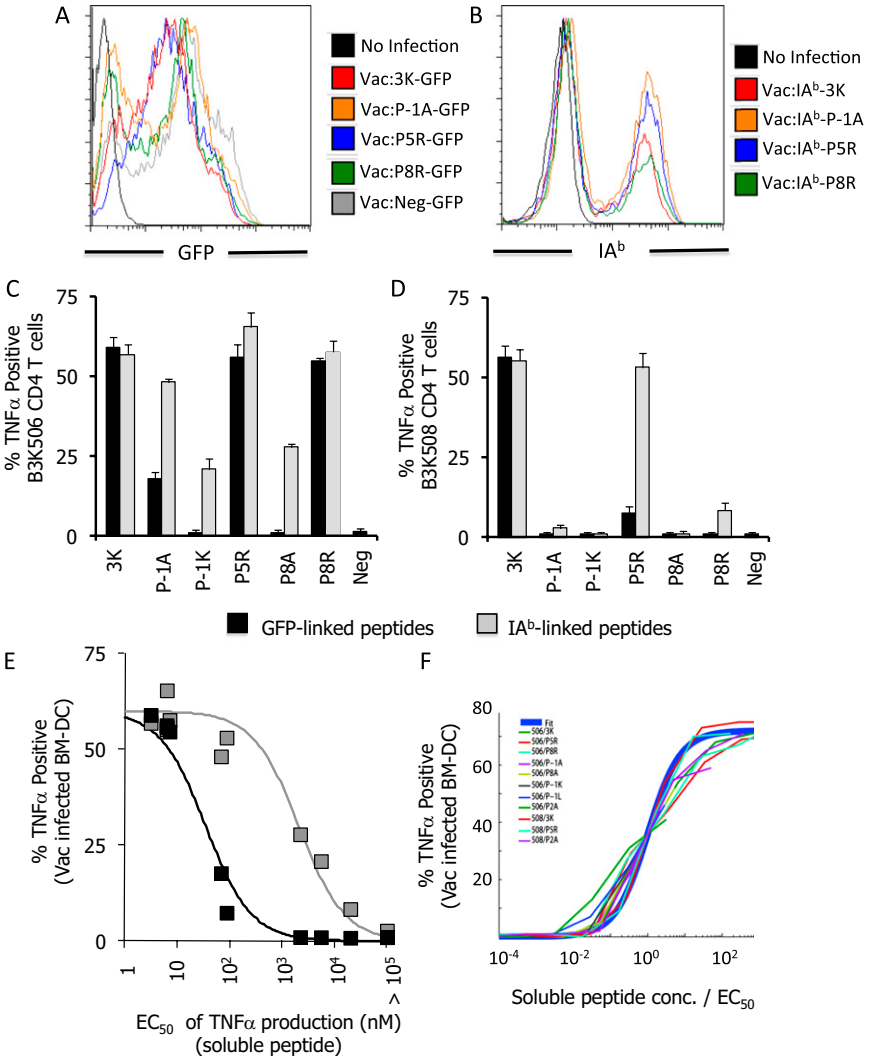

Fig. S1. BM-DCs infected with vaccinia viruses expressing 3K and 3K APLs fused to GFP or IA^b differentially activated naïve 3K-specific B3K506 and B3K508 CD4 T cells. (*A*) BM-DCs infected with Vac:peptide–GFP viruses express similar levels of GFP. (*B*) BM-DCs, differentiated from MHC class II-deficient mice that are infected with Vac:IA^b–peptide viruses, express similar levels of MHC class II. Naïve B3K506 T cells (*C*) or B3K508 T cells (*D*) were incubated with BM-DCs (differentiated from C57BL/6 mice) infected with Vac:peptide–GFP (black bars) or Vac:IA^b–peptide (gray bars) and analyzed for TNFα expression; 3K or 3K APL is listed on the *x* axis. Data are the average of three independent experiments. (*E*) The production of TNFα by naïve B3K506 and B3K508 T cells incubated with BM-DCs infected with Vac:peptide–GFP (black squares) and Vac:IA^b–peptide (gray squares) was compared with the concentration of soluble peptide that induces half-maximal TNFα production, i.e., the EC_{50} value (Table S1). The fit curves are described in *SI Materials and Methods*. (*F*) The parameters used in fitting viral potency are consistent with in vitro dose–response curves. T-cell dose–response curves (2) have a sigmoidal shape with respect to the logarithm of the peptide concentration. The fit is based on Eq. **S1** with measured EC_{50} values, treating peptide concentration as the independent variable. Fit parameters: r_{max} = 72%; n = 1.

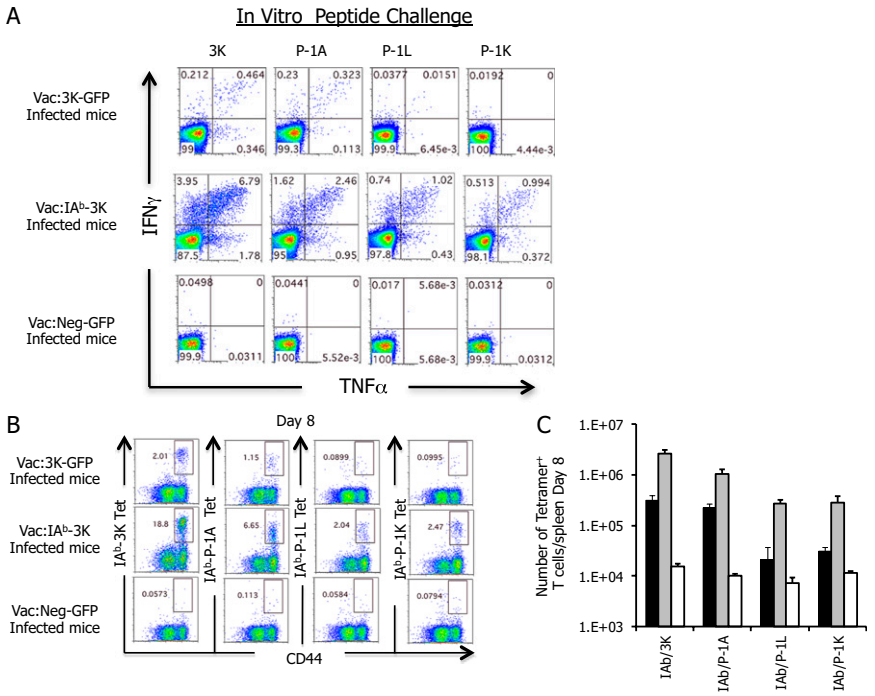

Fig. S2. Expansion of 3K-, P-1A–, P-1L–, and P-1K–reactive, IFNγ-producing and tetramer-positive CD4 T cells in the spleen of 506β mice 8 d postinfection. (*A*) Representative example of CD4 T cells from 506β mice infected with Vac:3K–GFP (top row), Vac:IA^b–3K (middle row), or Vac:Neg–GFP (bottom row) for the ability to produce IFNγ and TNFα following stimulation with 1 μg/mL 3K, P-1A, P-1L, or P-1K peptide. (*B*) CD4 T cells from 506β mice infected with Vac:3K–GFP (top row), Vac:IA^b–3K (middle row), or Vac:Neg–GFP (bottom row) were analyzed for the ability to be stained with IA^b–3K, –P-1A, –P-1L, or –P-1K tetramers. (*C*) Quantification of the total number of CD4 T cells per spleen that are stained with IA^b–3K, –P-1A, –P-1L, or –P-1K tetramer on day 8 following infection with Vac:3K–GFP (black bars), Vac:IA^b–3K (gray bars), or Vac:Neg–GFP (white bars). Data are the average of six total mice per group.

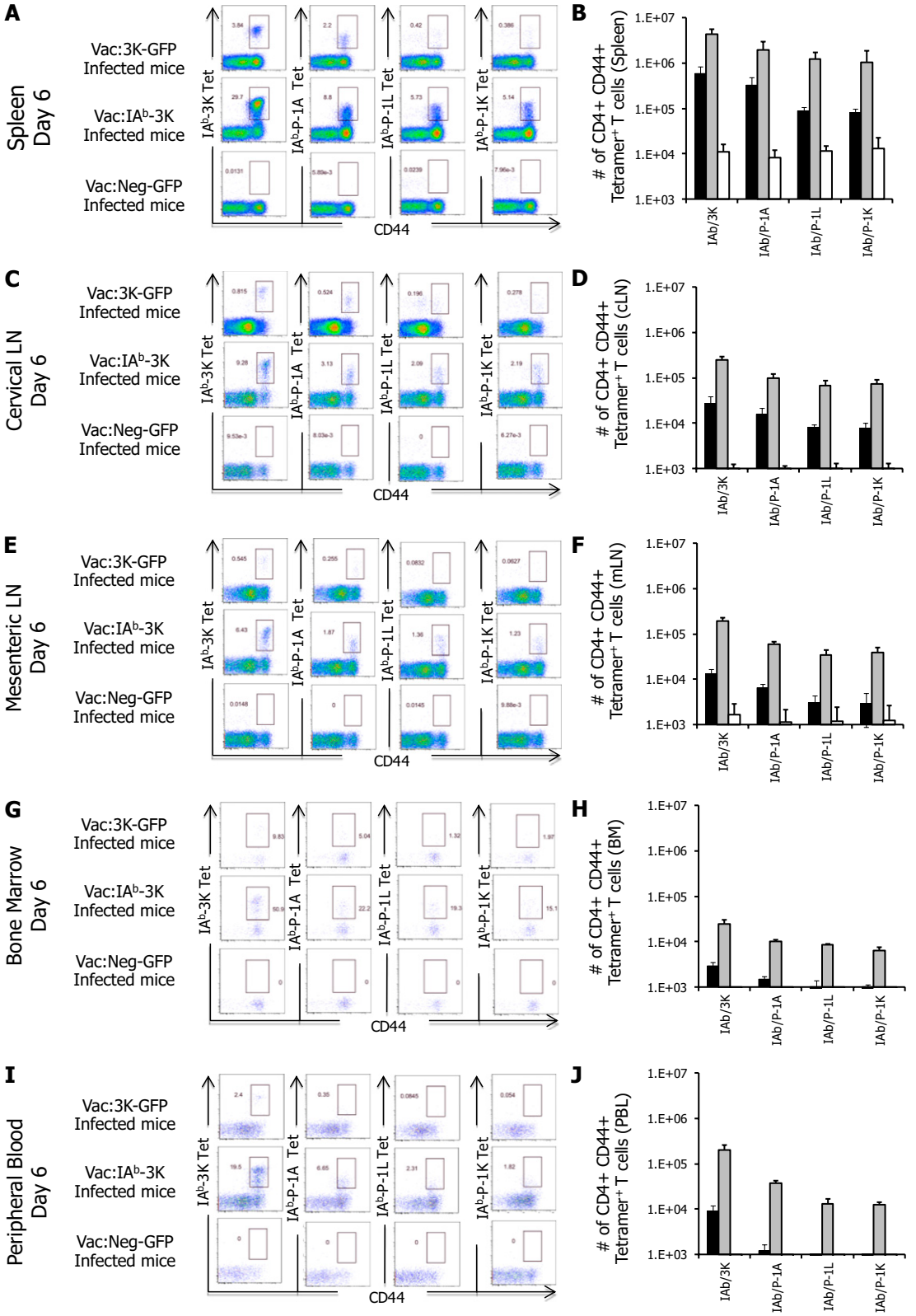

Fig. S3. CD4 T cells that are 3K, P-1A, P-1L, and P-1K tetramer-positive accumulate in the spleen and, to a lesser extent, in other secondary lymphoid organs on day 6 after vaccinia infection. (*A* and *B*) Mice (506β) were infected with Vac:3K–GFP (top row), Vac:IA^b–3K (middle row), or Vac:Neg–GFP (bottom row), and CD44+ CD4+ FACS-gated T cells isolated from the spleen of mice were stained with 1 μg/mL 3K, P-1A, P-1L, and P-1K tetramer (*A*) and quantified (*B*). For quantification, Vac:3K–GFP–infected mice are black solid bars, Vac:IA^b–3K–infected mice are gray solid bars, and Vac:Neg–GFP–infected mice are white solid bars. These same mice were analyzed for 3K, P-1A, P-1L, and P-1K tetramer-positive CD44+ CD4+ gated T cells present in the cervical lymph nodes (*C* and *D*), mesenteric lymph nodes (*E* and *F*), bone marrow (*G* and *H*), and peripheral blood (*I* and *J*). For blood quantification, it was assumed a 20-g mouse has 1.5 mL of blood. Data are representative of average of four mice per group.

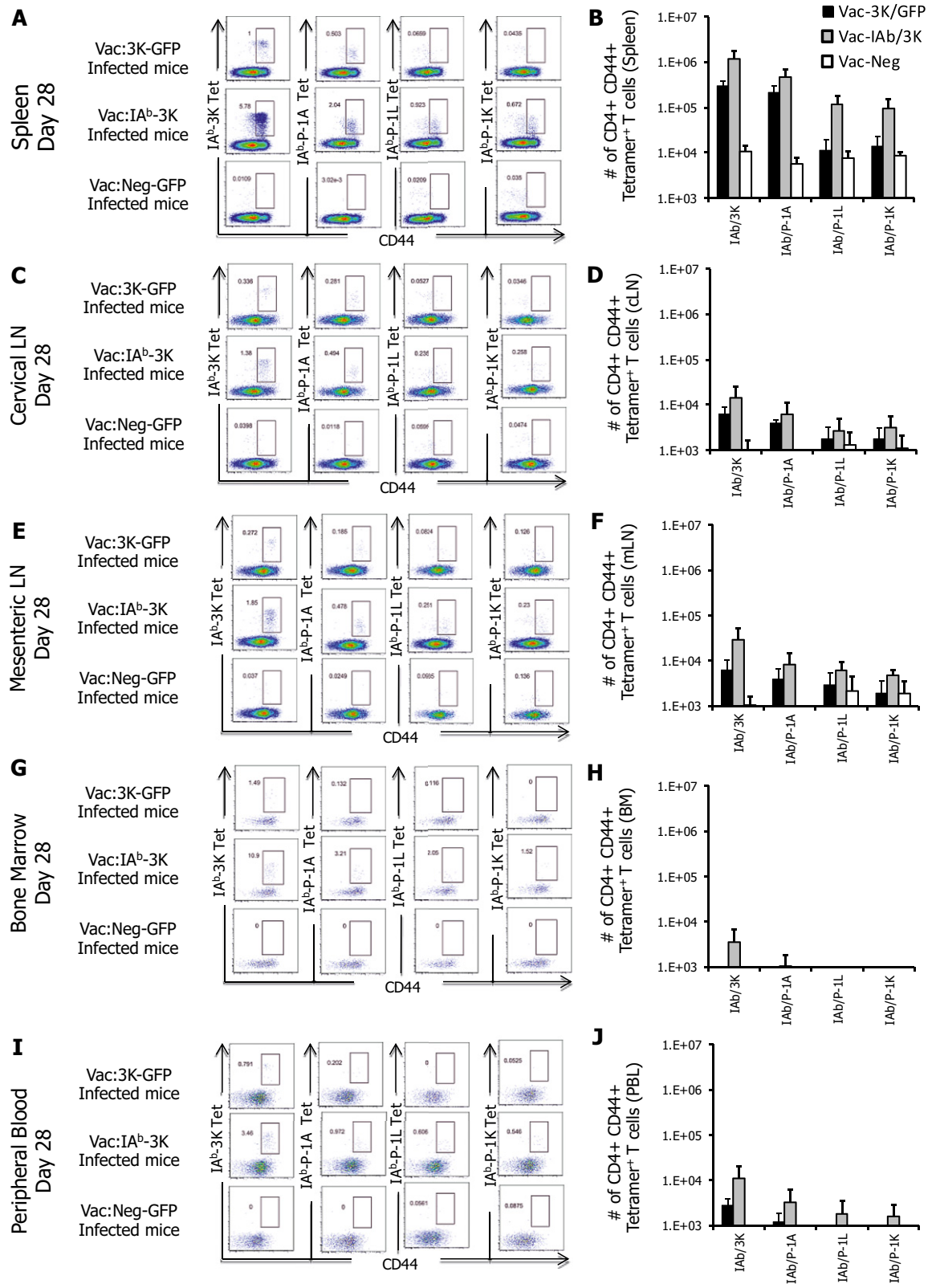

Fig. S4. CD4 T cells that are 3K, P-1A, P-1L, and P-1K tetramer-positive accumulate in the spleen and, to a lesser extent, in other secondary lymphoid organs on day 28 after vaccinia infection. (*A* and *B*) Mice (506β) were infected with Vac:3K–GFP (top row), Vac:IA^b–3K (middle row), or Vac:Neg–GFP (bottom row), and CD44+ CD4+ FACS-gated T cells isolated from the spleen of mice were stained with 1 μg/mL 3K-, P-1A, P-1L, and P-1K tetramer (*A*) and quantified (*B*). For quantification, Vac:3K–GFP–infected mice are black solid bars, Vac:IA^b–3K–infected mice are gray solid bars, and Vac:Neg–GFP–infected mice are white solid bars. These same mice were analyzed for 3K, P-1A, P-1L, and P-1K tetramer-positive CD44+ CD4+ gated T cells present in the cervical lymph nodes (*C* and *D*), mesenteric lymph nodes (*E* and *F*), bone marrow (*G* and *H*), and peripheral blood (*I* and *J*). For blood quantification, it was assumed a 20-g mouse has 1.5 mL of blood. Data are representative of average of five mice per group.

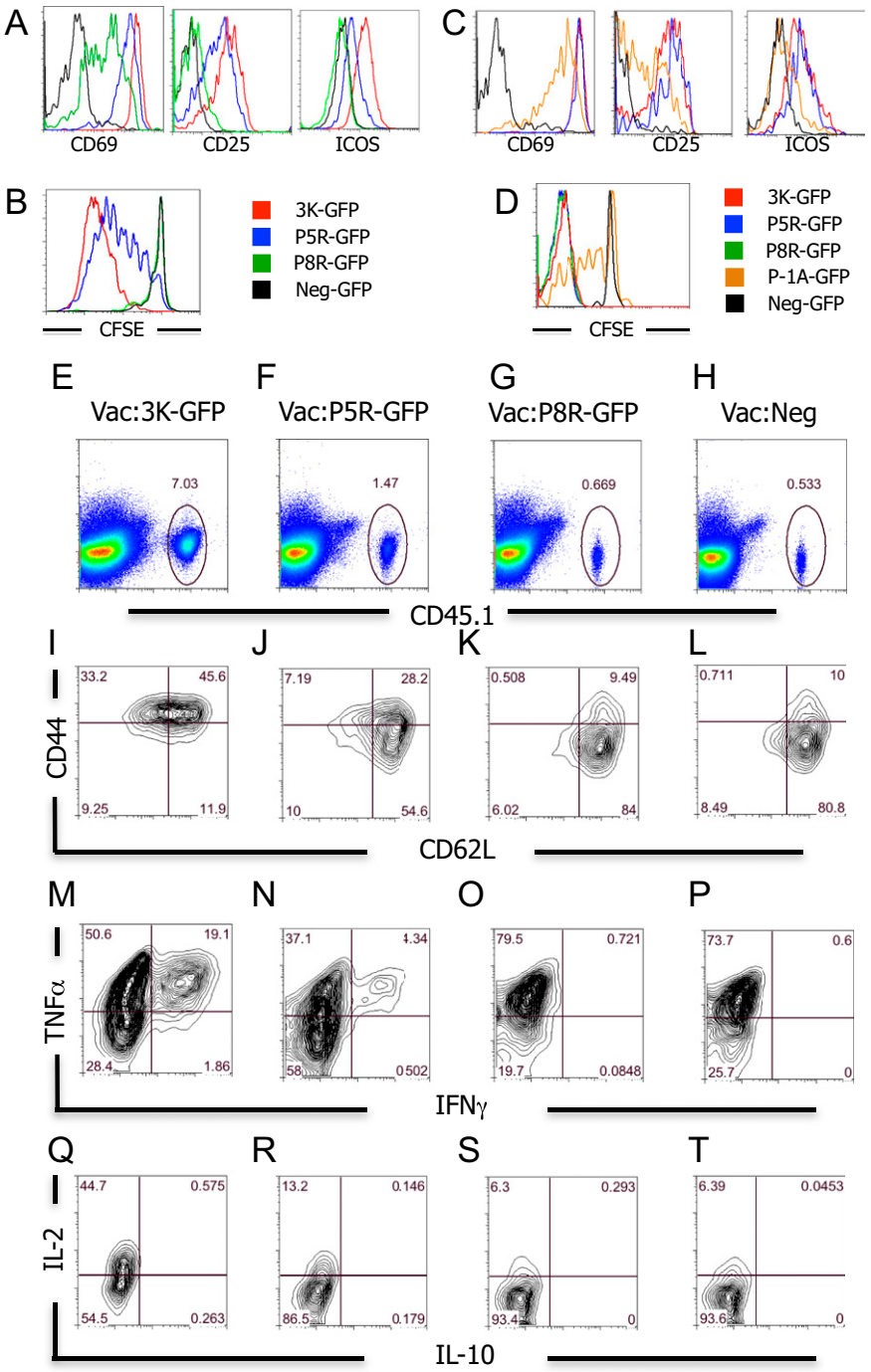

Fig. S5. Infection of mice with Vac:peptide–GFP virus induces three categories of early CD4 T-cell response: weak-potency ligands induce the expression of T-cell surface markers associated with activation but fail to induce proliferation; medium-potency ligands induce the expression of activation markers at an intermediate level and modest proliferation; strong-potency ligands induce robust expression of activation markers and T-cell proliferation. (*A*) B6.CD45.1$^+$ B3K508 T cells (1×10^6) were transferred into C57BL/6 mice and infected with Vac:3K–GFP (strong potency, red), Vac:P5R–GFP (medium potency, blue), Vac:P8R–GFP (weak potency, green), or Vac:Null–GFP (null potency, black) virus. B3K508 CD4 T cells were analyzed 18 h postinfection for the expression of CD69 or 48 h postinfection for the expression of CD25 and ICOS. (*B*) B3K508 T cells labeled with CFSE were analyzed for cellular proliferation 3 d after infection. Data are representative of six mice per group. (*C*) B6.CD45.1$^+$ B3K506 T cells (1×10^6) were transferred into C57BL/6 mice and infected with Vac:3K–GFP (strong potency, red), Vac:P5R–GFP (strong potency, blue), Vac:P8R–GFP (strong potency, green), Vac:P-1A–GFP (medium potency, orange), or Vac:Null–GFP (null potency, black) virus. B3K506 CD4 T cells were analyzed 18 h postinfection for the expression of CD69 or after 48 h for the expression of CD25 and ICOS. (*D*) B3K506 T cells labeled with CFSE were analyzed for cellular proliferation 3 d after infection. Data are representative of six mice per group. (*E*–*T*) Three days after Vac:peptide–GFP virus infection carrying weak-, medium-, and strong-potency ligands, B3K508 CD4 T cells show distinct changes in the activation markers, CD44 and CD62L, and have a differential ability to produce IFNγ. B6.CD45.1$^+$ B3K508 T cells (1×10^6) were transferred into C57BL/6 mice and infected with Vac:3K–GFP (strong potency, column 1) (*E*), Vac:P5R–GFP (medium potency, column 2) (*F*), Vac:P8R–GFP (weak potency, column 3) (*G*), or Vac:Null–GFP (null potency, column 4) (*H*) virus. Seventy-two hours postinfection, B3K508 CD4 T cells were identified using the congenic marker, CD45.1, and analyzed for the expression of CD44 and CD62L (*I*–*L*) or for the ability to produce IFNγ and TNFα (*M*–*P*) or IL-2 and IL-10 (*Q*–*T*). Data are representative of four mice per group.

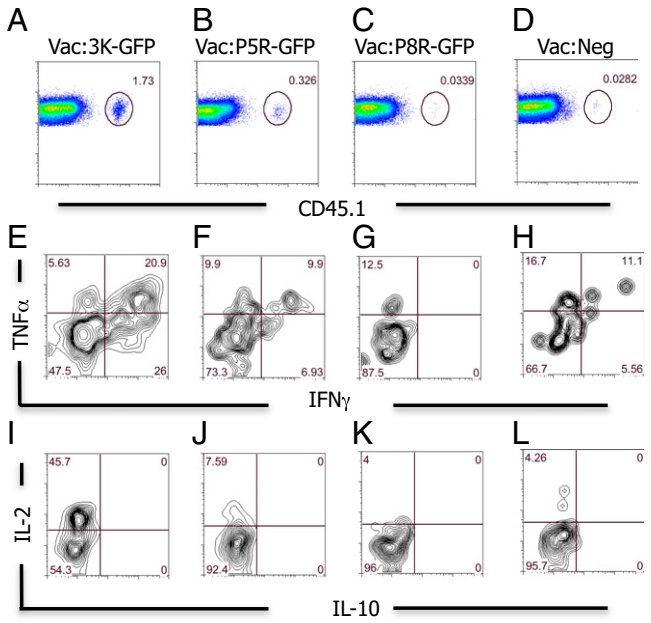

Fig. S6. Seven days after Vac:peptide–GFP virus infection, activated B3K508 CD4 T cells are strong producers of IFNγ, TNFα, and IL-2 when the virus carries a strong potency ligand. B6.CD45.1$^+$ B3K508 T cells (1×10^5) were transferred into C57BL/6 mice and infected with Vac:3K–GFP (strong potency, column 1) (*A*), Vac:P5R–GFP (medium potency, column 2) (*B*), Vac:P8R–GFP (weak potency, column 3) (*C*), or Vac:Null–GFP (null potency, column 4) (*D*) virus. Seven days postinfection, B3K508 CD4 T cells were identified using the congenic marker, CD45.1, and analyzed for the ability to produce IFNγ and TNFα (*E*–H) or IL-2 and IL-10 (*I*–*L*). Data are representative of six mice per group.

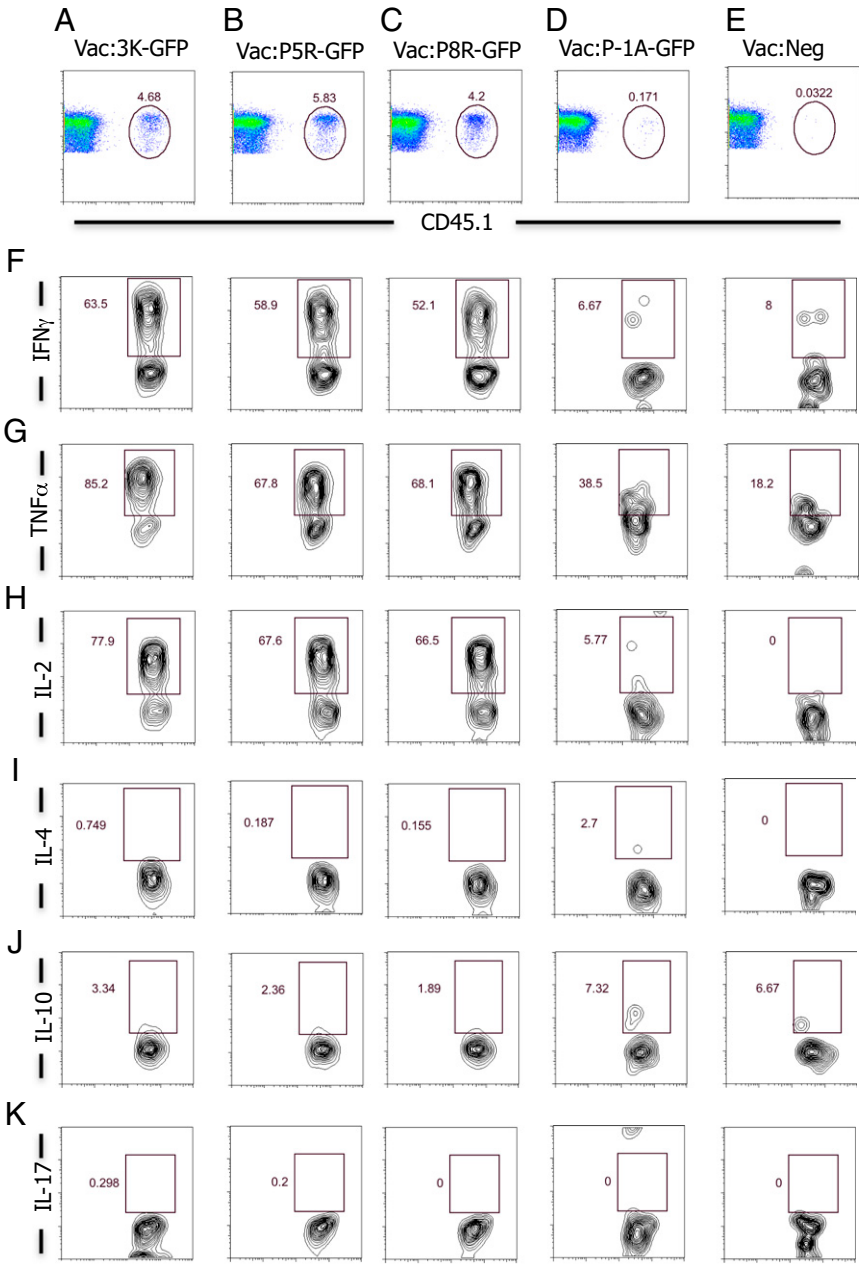

Fig. S7. Seven days after Vac:peptide–GFP virus infection, activated B3K506 CD4 T cells are strong producers of IFNγ, TNFα, and IL-2 when the virus carries a strong potency ligand. B6.CD45.1$^+$ B3K506 T cells (1×10^5) were transferred into C57BL/6 mice and infected with Vac:3K–GFP (strong potency, column 1) (*A*), Vac:P5R–GFP (strong potency, column 2) (*B*), Vac:P8R–GFP (strong potency, column 3) (*C*), Vac:P-1A–GFP (medium potency, column 4) (*D*), or Vac:Null–GFP (null potency, column 5) (*E*) virus. Seven days postinfection, B3K506 CD4 T cells were identified using the congenic marker, CD45.1, and analyzed for the ability to produce IFNγ (row *F*), TNFα (row *G*), IL-2 (row *H*), IL-4 (row *I*), IL-10 (row *J*), or IL-17 (row *K*). Data are representative of four mice per group.

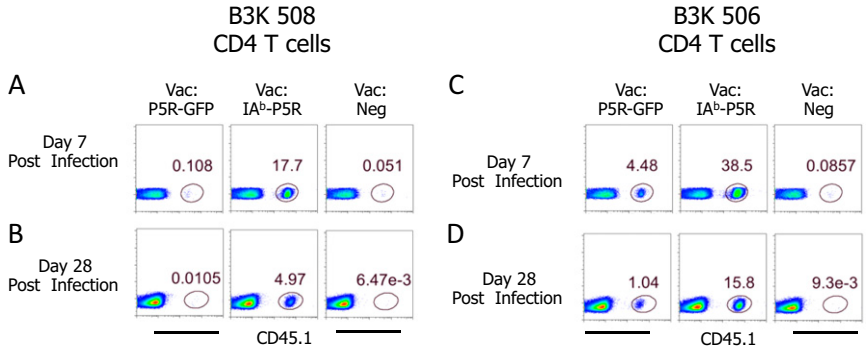

Fig. S8. Infection of mice with Vac:IA^b-linked peptides allows medium-potency ligands to induce massive expansion and maintenance CD4 T cells. (*A* and *B*) CD45.1$^+$ B3K508 CD4 T cells (1×10^5) were transferred into C57BL/6 mice and infected with the medium potency peptide, P5R, fused to GFP (Vac:P5R–GFP, column 1), IA^b (Vac:IA^b–P5R, column 2), or Vac:Neg (column 3). At 7 d (*A*) or 28 d (*B*) postinfection, the B3K508 CD4 T cells were identified from spleen cells of infected mice as CD8^{neg}, MHC CL2^{neg}, Thy1.2$^+$, CD4$^+$, CD45.1$^+$ cells. FACS plots are shown comparing endogenous CD4 T cells (CD45.1^{neg}) with B3K508 CD4 T cells (CD45.1$^+$). Note the massive increase of B3K508 T cells in the spleen of infected mice following Vac:IA^b–P5R infections compared with Vac:P5R–GFP infections on both day 7 and day 28. Data are representative of six mice per group. (*C* and *D*) As a control for the P5R viruses, 1×10^5 CD45.1$^+$ B3K506 CD4 T cells were transferred into C57BL/6 mice and infected with the same Vac:P5R–GFP (column 1), Vac:IA^b–P5R (column 2), or Vac:Neg (column 3) virus. The P5R peptide is a strong potency ligand for the B3K506 T cells. Note the increase in expansion (day 7) and maintenance (day 28) of B3K506 T cells responding to Vac:P5R–GFP infection, compared with B3K508 T cells responding to the same Vac:P5R–GFP virus infection. Data are representative of six mice per group.

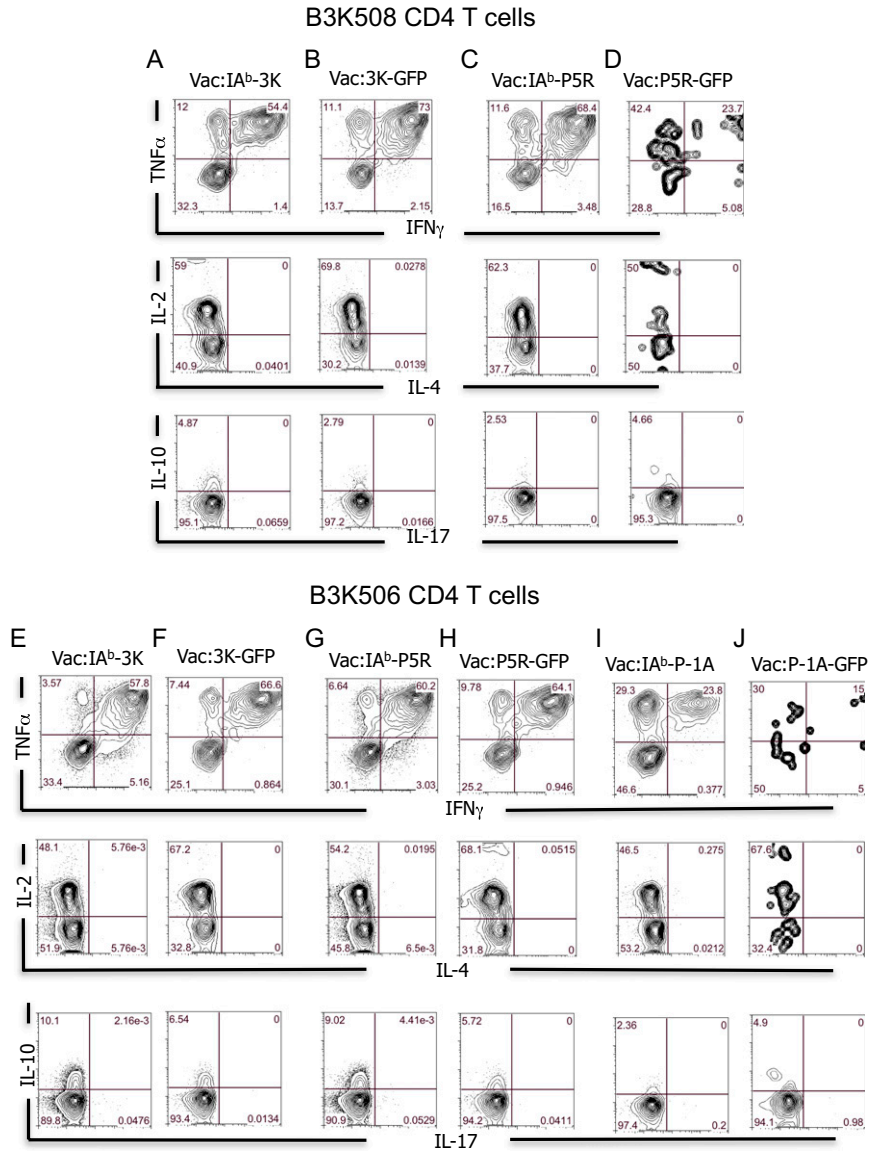

Fig. S9. CD4 T cells responding to Vac:IA^b-linked peptide infections carrying medium-potency ligands are strong producers of IFNγ, TNFα, and IL-2. (*A–D*) CD45.1$^+$ B3K508 CD4 T cells (1×10^5) were transferred into C57BL/6 mice. Recipient mice were infected with either the strong-potency peptide, 3K, fused to IA^b (Vac:IA^b–3K, column 1) (*A*) or fused to GFP (Vac:3K–GFP, column 2) (*B*), or the medium-potency peptide, P5R, fused to IA^b (Vac:IA^b–P5R, column 3) (*C*) or fused to GFP (Vac:P5R–GFP, column 4) (*D*). Seven days after infection, CD45.1$^+$ B3K508 CD4 T cells were analyzed for the ability to produce IFNγ and TNFα (row 1), IL-4 and IL-2 (row 2), and IL-17A and IL-10 (row 3). Note the strong IFNγ production by B3K508 CD4 T cells responding to Vac:IA^b–P5R infection. Data are representative of four mice per group. (*E–J*) CD45.1$^+$ B3K506 CD4 T cells (1×10^5) were transferred into C57BL/6 mice. Recipient mice were infected with either the strong-potency peptide, 3K, fused to IA^b (Vac:IA^b–3K, column 1) (*E*) or fused to GFP (Vac:3K–GFP, column 2) (*F*), the strong-potency peptide, P5R, fused to IA^b (Vac:IA^b–P5R, column 3) (*G*) or fused to GFP (Vac:P5R–GFP, column 4) (*H*), or the medium potency peptide, P-1A, fused to IA^b (Vac:IA^b–P-1A, column 5) (*I*) or fused to GFP (Vac:P-1A–GFP, column 6) (*J*). Seven days postinfection, CD45.1$^+$ B3K506 CD4 T cells were analyzed for the ability to produce IFNγ and TNFα (row 1), IL-4 and IL-2 (row 2), and IL-17A and IL-10 (row 3). Note the strong IFNγ production by B3K506 CD4 T cells responding to Vac:IA^b–P-1A infection. Data are representative of four mice per group.

Table S1. TCR-pMHC–binding parameters and T-cell expansion size following vaccinia infections

TCR	IA^b + 3K APL	K_D (μM)	k_a [1/(s × M)]	k_d (1/s)	$t_{1/2}$ (s)	t_a*	t_a**	TNFα EC_{50} (nM)	Prolif. EC_{50} (nM)	No. of T cells on D7 Vac:GFP	SD	No. of T cells on D7 Vac:IA^b	SD	No. of T cells on D28 Vac:GFP	SD	No. of T cells on D28 Vac:IA^b	SD
B3K506	WT	7	101,918	0.7	0.9	3.1	2.7	3.1	0.2	414,218	242,334	5,590,687	3,045,605	303,437	56,682	2,884,693	741,567
B3K506	P-1A	26	101,731	2.6	0.3	0.9	0.7	68	9	3,314	1,715	2,561,640	1,085,543	2,963	1,428	694,038	230,595
B3K506	P5R	11	74,654	0.8	0.9	2.3	1.9	6	0.2	422,836	182,084	4,216,339	2,073,190	273,105	73,719	2,647,031	919,696
B3K506	P8R	13	64,318	0.8	0.8	2.1	1.8	7	0.3	319,989	144,777	4,082,395	1,808,778	225,663	41,534	2,911,135	583,145
B3K508	WT	29	10,887	0.3	2.2	2.8	2.8	6	0.4	299,249	163,077	4,189,068	1,390,348	146,340	45,593	1,688,821	597,863
B3K508	P-1A	>550	ND	ND	ND	0.1	0.1	$>10^4$	10,000	1,912	733	5,579	4,227	876	717	1,539	765
B3K508	P5R	93	11,048	1.0	0.7	0.9	0.8	87	15	14,277	5,193	2,028,295	631,288	2,211	1,150	824,807	195,536
B3K508	P8R	>550	ND	ND	ND	0.1	0.1	20,000	980	2,853	2,371	12,657	3,766	731	802	7,594	2,141

K_D, k_a, k_d, $t_{1/2}$, t_a*, t_a**, and TNFα EC_{50} and proliferation (prolif.) EC_{50} were reported in ref. 2. t_a* is based on k_{on}* = 45,000 $\mu m^2/s$; t_a** is based k_{on}* = 60,000 $\mu m^2/s$.